Electronic Supplementary Material (ESI) for Soft Matter.
This journal is © The Royal Society of Chemistry 2021

Supplementary information

Silk granular hydrogels self-reinforced with regenerated silk fibroin fibers

Céline Samira Wyss,[a] Peyman Karami,[b] Adrien Demongeot,[a] Pierre-Etienne Bourban *[a] and Dominique P. Pioletti*[b]

[a] *Laboratory for Processing of Advanced Composites (LPAC), Ecole Polytechnique Fédérale de Lausanne (EPFL), CH-1015, Lausanne, Switzerland. * Email: pierre-etienne.bourban@epfl.ch*
[b] *Laboratory of Biomechanical Orthopedics (LBO), Ecole Polytechnique Fédérale de Lausanne (EPFL), CH-1015, Lausanne, Switzerland.*

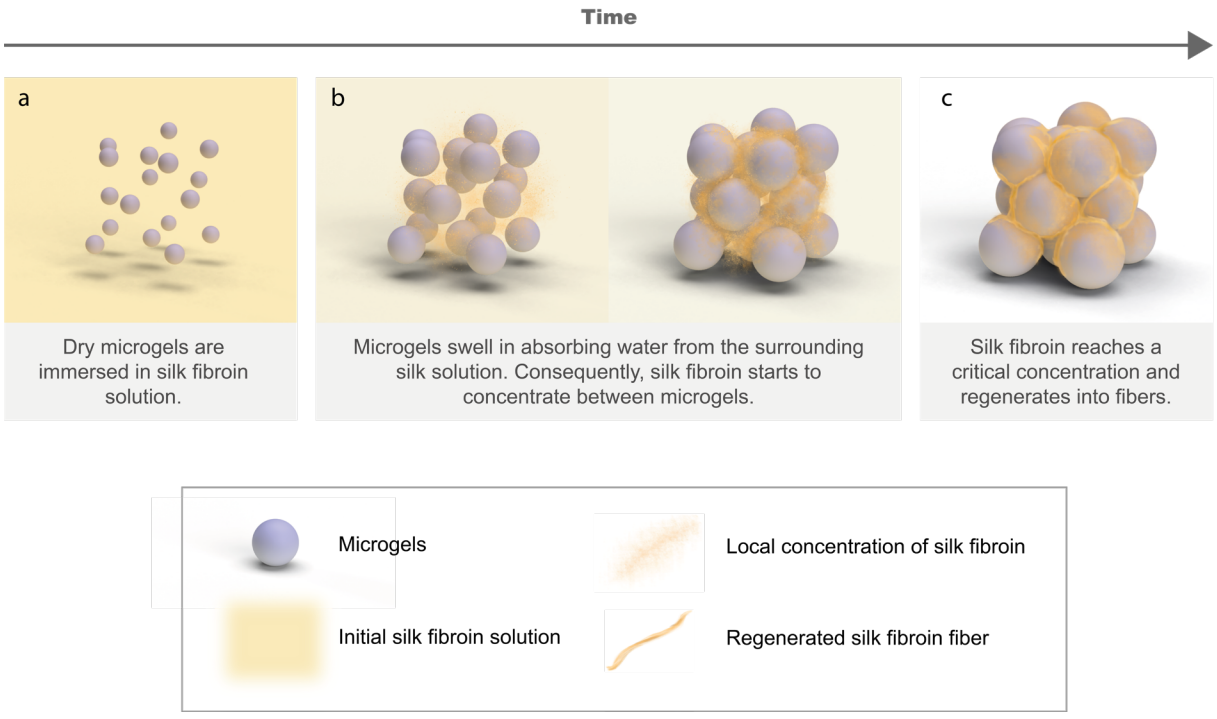

Table of contents

1. Supplementary materials and methods

1.1. Microgel synthesis

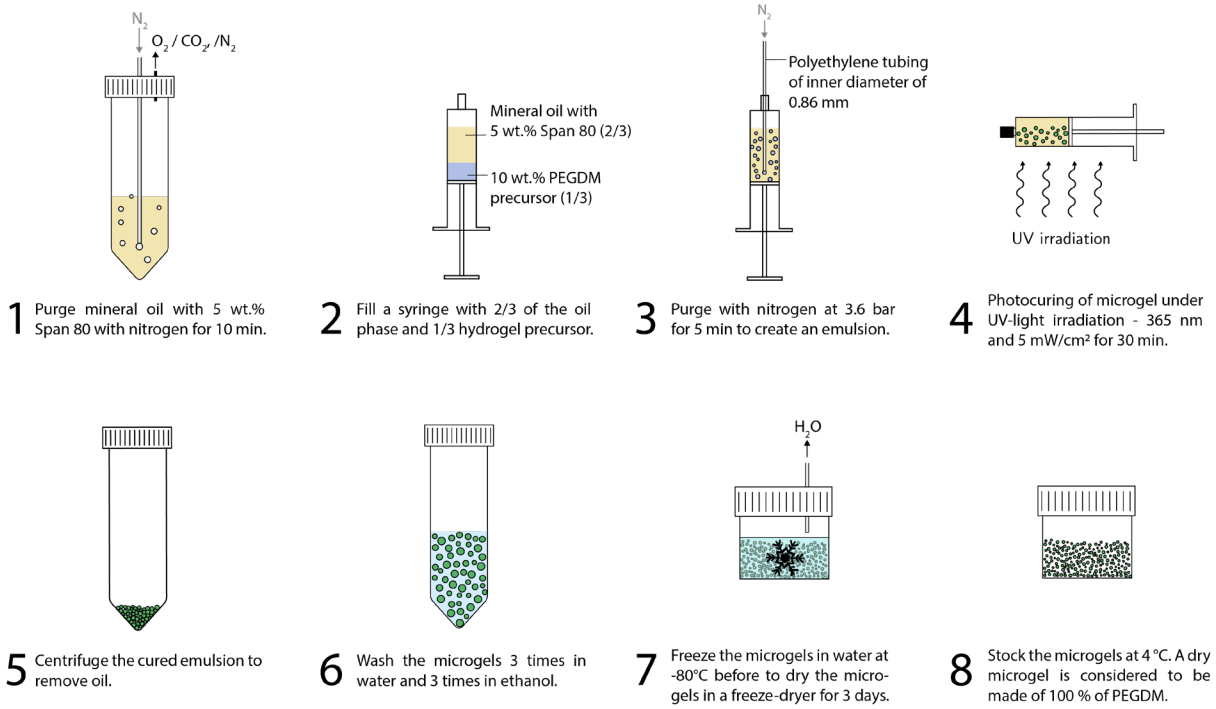

1 Purge mineral oil with 5 wt.% Span 80 with nitrogen for 10 min.

2 Fill a syringe with 2/3 of the oil phase and 1/3 hydrogel precursor.

3 Purge with nitrogen at 3.6 bar for 5 min to create an emulsion.

4 Photocuring of microgel under UV-light irradiation - 365 nm and 5 mW/cm² for 30 min.

5 Centrifuge the cured emulsion to remove oil.

6 Wash the microgels 3 times in water and 3 times in ethanol.

7 Freeze the microgels in water at -80°C before to dry the microgels in a freeze-dryer for 3 days.

8 Stock the microgels at 4 °C. A dry microgel is considered to be made of 100 % of PEGDM.

Fig. S1: Microgels synthesis

1.2. Water-based silk fibroin solution preparation

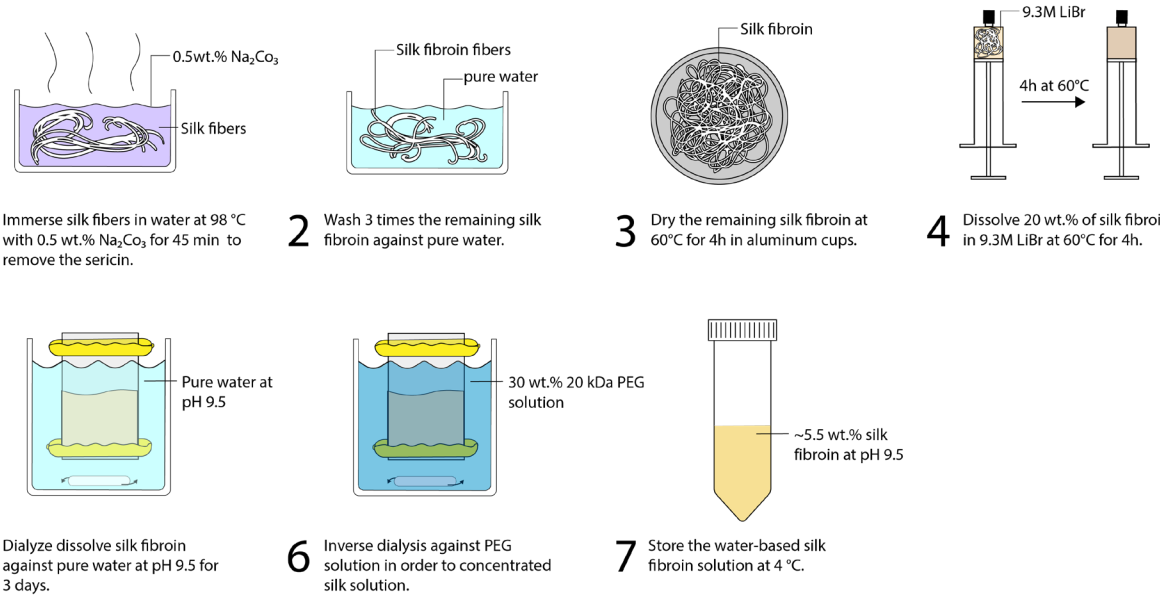

1 Immerse silk fibers in water at 98 °C with 0.5 wt.% Na_2Co_3 for 45 min to remove the sericin.

2 Wash 3 times the remaining silk fibroin against pure water.

3 Dry the remaining silk fibroin at 60°C for 4h in aluminum cups.

4 Dissolve 20 wt.% of silk fibroin in 9.3M LiBr at 60°C for 4h.

5 Dialyze dissolve silk fibroin against pure water at pH 9.5 for 3 days.

6 Inverse dialysis against PEG solution in order to concentrated silk solution.

7 Store the water-based silk fibroin solution at 4 °C.

Fig. S2: Preparation of water based silk fibroin solution

1.3. Silk granular hydrogel synthesis

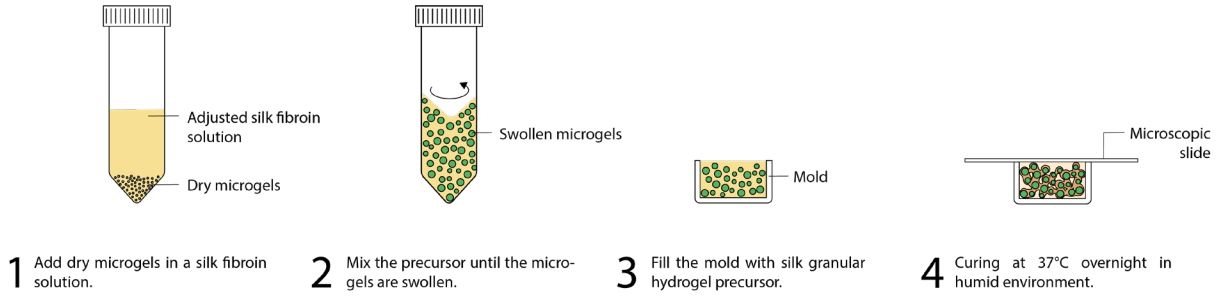

Fig. S3: Synthesis of silk granular hydrogels.

1.4. Synthesis rule for silk granular hydrogel

Silk granular hydrogels initially containing 4 wt.% of dry microgels had the lowest swelling ratios. However, for load-bearing applications, those composed of 5 wt.% of dry microgels would present a better compromise between mechanical and swelling properties due to their higher elastic moduli. The material properties of silk granular hydrogels can be extended by using other types of microgels. Nevertheless, it is not straightforward to determine the initial dry microgels concentration, because their water uptake significantly depends on the material (*i.e.* polymer hydrophilicity, polymer concentration, molecular weight, crosslinking density). Therefore, based on the observations made in this study, a synthesis method for selecting the initial concentration of dry microgels is proposed and explained in Fig. S4. The method estimates first the water uptake of the dry microgels with an equivalent neat hydrogel cylinder. For example, when a swollen PEGDM hydrogel had a final polymer content of 4 wt.% it was observed that adding 1 wt.% more of polymer into the dry microgels was ideal for the regeneration of silk fibroin. The addition of less or more than 1 wt.% regenerated a to loosely or to compact granular structure inhibiting the adequate formation of silk fibers.

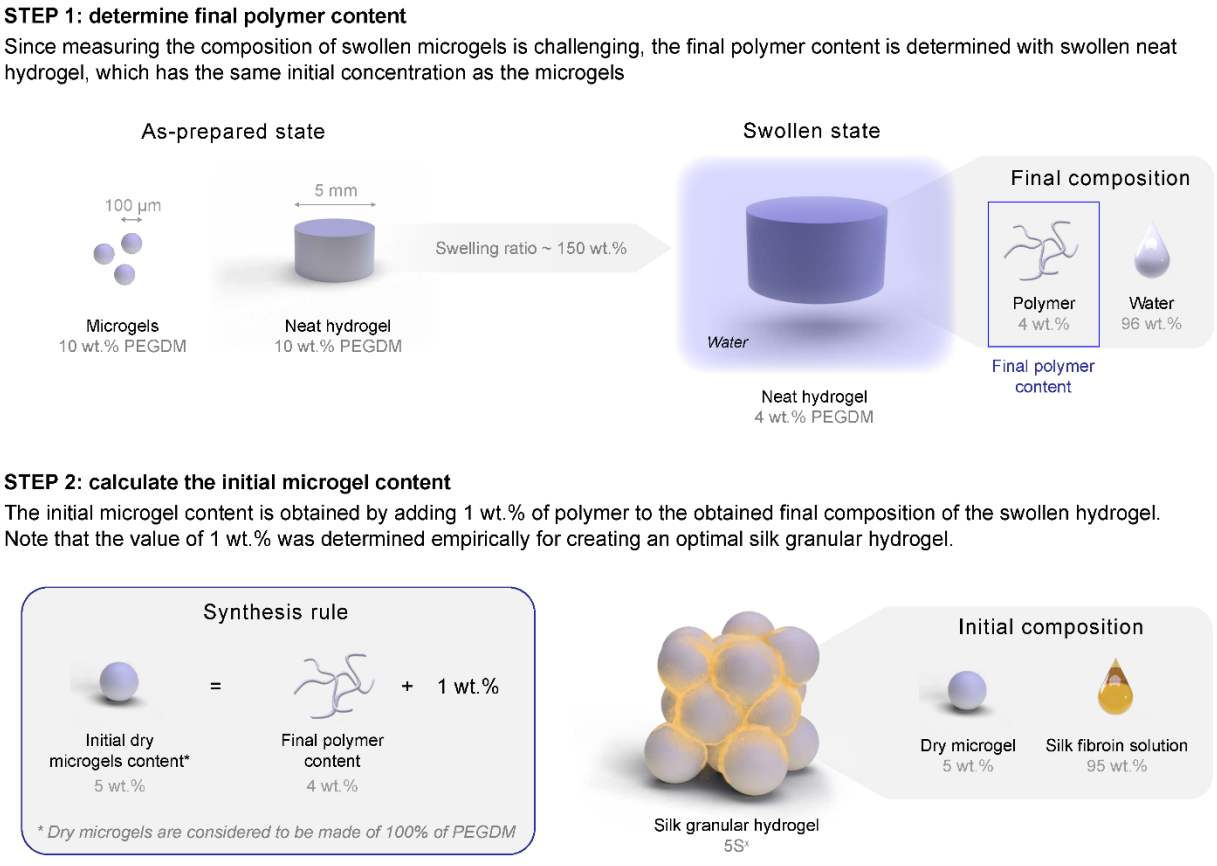

Fig. S4: Synthesis rule for creating silk granular hydrogel

2. Supplementary results

2.1. Tensile properties of different hydrogel structures

For completing the mechanical characterization, tensile properties were evaluated and presented in Fig. S5, which is a property chart that presents the tensile modulus, determined between 10% and 15% applied strain, as a function of strain at failure. The tensile moduli of silk granular hydrogels (*i.e.* 86-296 kPa) were significantly larger than hydrogel composite - *C* (*i.e.* 39-105 kPa) or hybrid granular hydrogel - *H* (*i.e.* 27-90 kPa). However, as observed in many other materials, an increase in stiffness is mostly accompanied by a decrease in elongation. The average strains measured at failure (*i.e.* 29-62%) were dramatically smaller than the other structures. The lower elongations were probably driven by the maximal extension of regenerated silk fibroin itself. Indeed, it was reported that the elongation of regenerated silk fibroin hardly exceeds 65%[1].

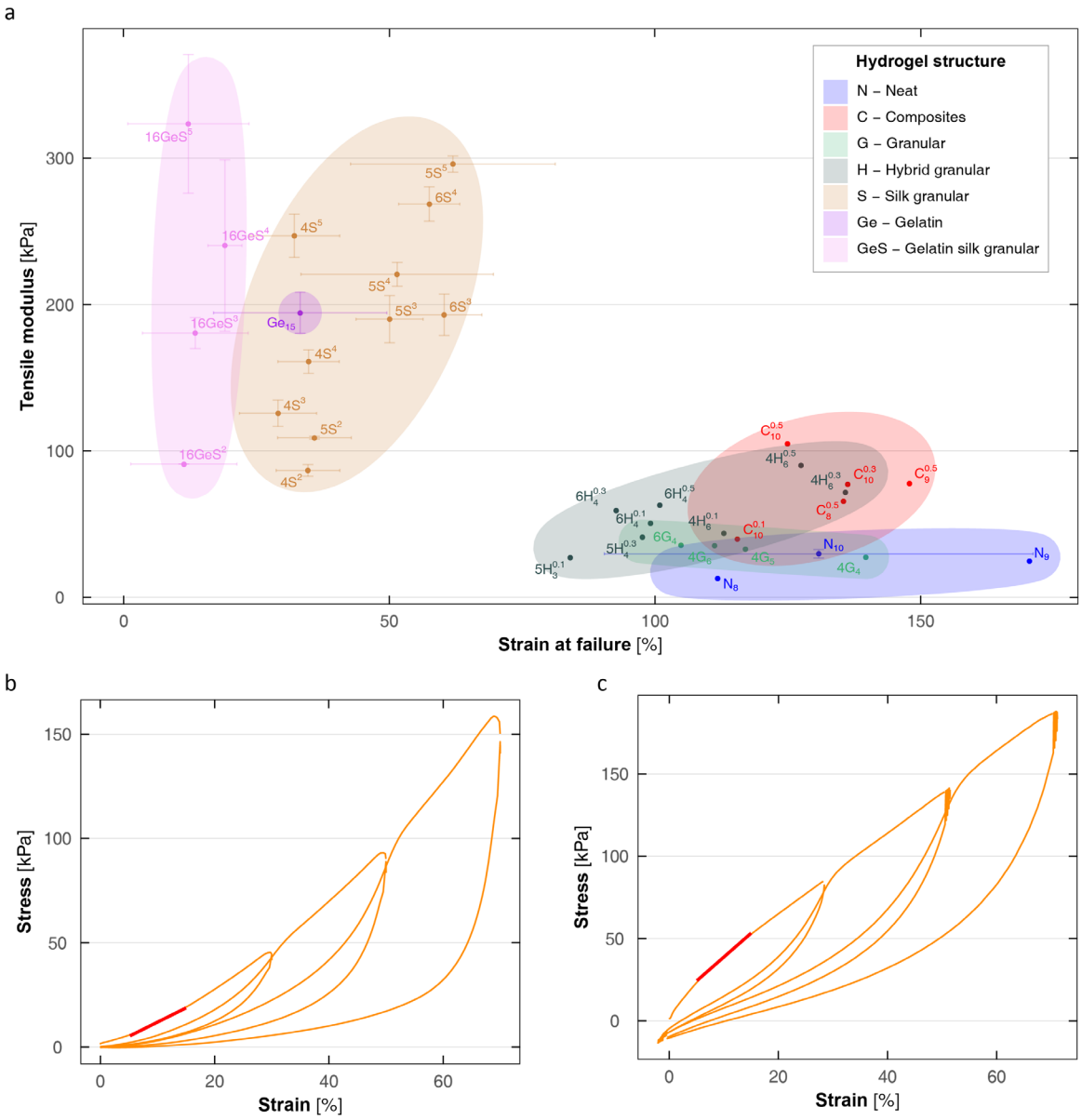

Fig. S5: (a) Property chart of seven different hydrogel structures with various compositions showing the tensile modulus determined between 10% and 15% applied strain as a function of the strain at failure. Representative cyclic loadings in (b) compression and (c) tensile of silk granular hydrogel - $5S^5$.

2.2. Microstructures

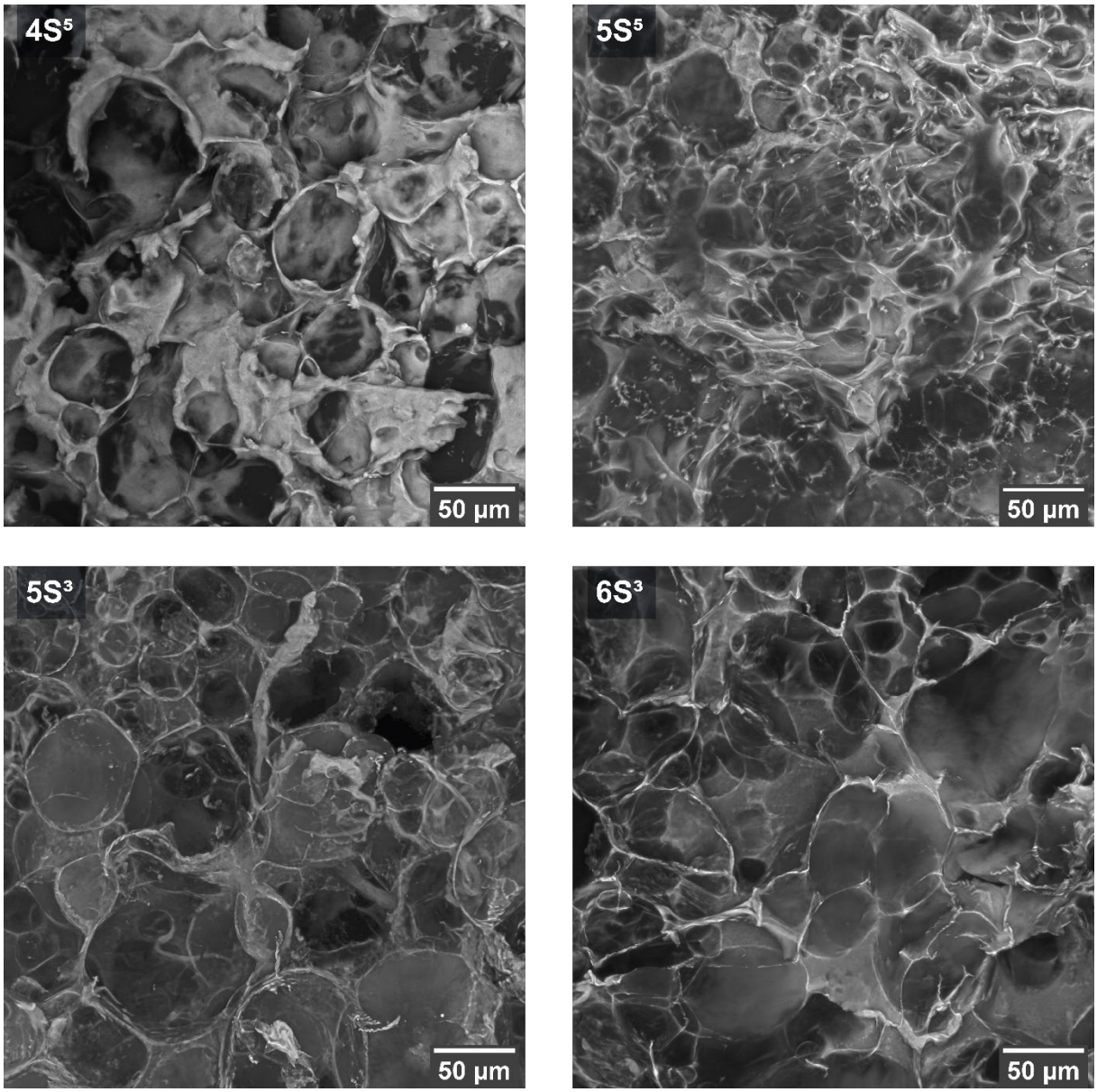

Fig. S6: Microstructures of 4 different silk granular hydrogels compositions.

2.3. Silk fibroin crystallinity

2.3.1. Representative FTIR spectra of silk fibroin and silk granular hydrogels

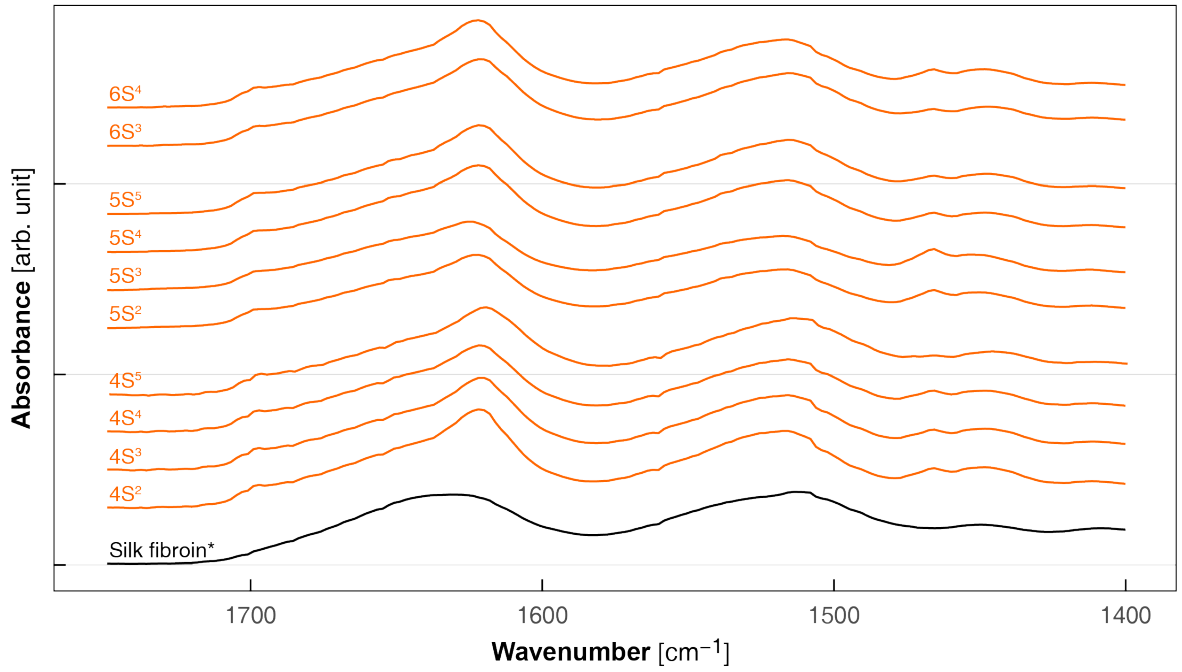

Fig. S7: FTIR of silk fibroin fibers regenerated *in situ* in tested silk granular hydrogels. *Silk fibroin solution was dried for 2h at 60°C.

2.3.2. Assignment of absorbance peaks to secondary structures of silk fibroin

Table S1: Absorbance peaks of secondary structures of silk fibroin [1–5]

Secondary structure	Wavelength [cm^{-1}]
Side chains	1605-1615
β-sheet (weak) / aggregate β-strand	1616-1621
Parallel β-sheet	1620
Anti-parallel β-sheet	1623
β-sheet (strong)	1618, 1621-1638
Random coil	1638-1654
α-helices	1655-1662
β-turns	1663-1696, 1715
β-sheet (weak)	1697-1703

2.3.3. Deconvolution of FTIR spectra

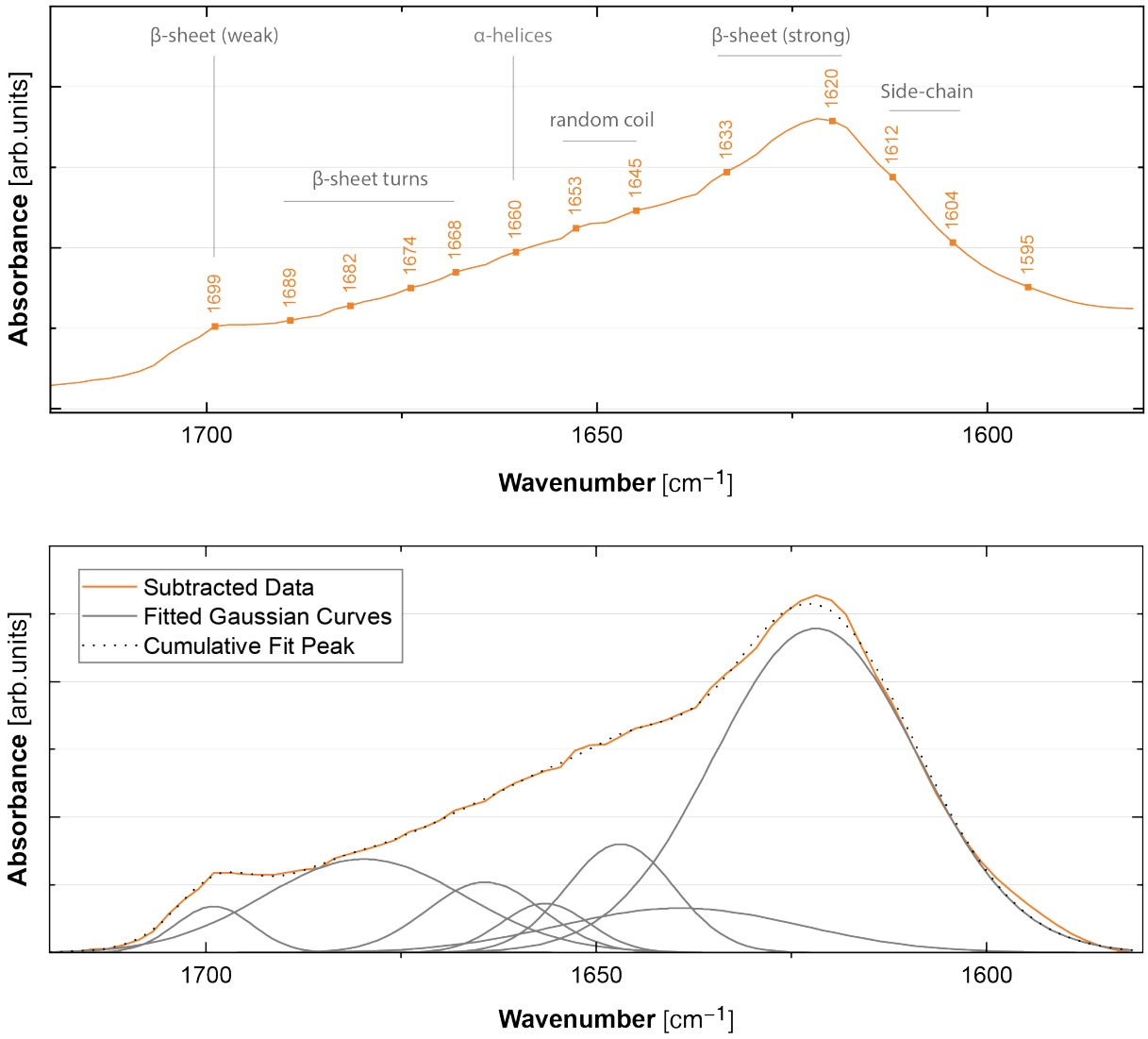

Fig. S8: Secondary structures of silk fibroin regenerate in silk granular hydrogel. (a) Hidden peaks were revealed by the second derivative of the convoluted IR spectra of silk granular hydrogel – 5S[5]. (b) Deconvolution of FTIR spectra using Gaussian curves of silk granular hydrogel - 5S[5].

Table S2: Assigned secondary structures of silk granular hydrogel - $5S^5$ determined from deconvoluted Gaussian curves from FTIR Spectra.

Peak ID	Peak center [cm^{-1}]	Peak area [cm^{-1}]	Peak area [%]	Secondary structure
1	1622	15.6	53.5	β-sheet (strong)
2	1639	2.6	8.8	Random coil
3	1647	2.8	9.5	Random coil
4	1657	1	3.5	α-helices
5	1664	1.9	6.6	β-turns
6	1680	4.4	15.2	β-turns
7	1699	0.8	2.9	β-sheet (weak)

Table S3: Assigned secondary structures of dry silk fibroin determined from deconvoluted Gaussian curves from FTIR Spectra.

Peak ID	Peak center [cm^{-1}]	Peak area [cm^{-1}]	Peak area [%]	Secondary structure
1	1618	11.5	40.1	β-sheet (weak) / aggregate β-strand
2	1645	11.2	39.1	Random coil
3	1653	1.6	5.6	Random coil
4	1664	0.7	2.4	β-turns
5	1676	0.5	1.7	β-turns
6	1686	3.2	11.1	β-turns

2.4. Mechanical gradient through sequential layering

Hydrogels can currently not compete with some load-bearing tissues, such as meniscus or articular cartilage, mainly because it is difficult to mimic their highly hierarchical microstructures. For example, as illustrated in Fig. S9, articular cartilage exhibits multiple mechanical gradients. The stiffness progressively increases when approaching the subchondral bone and regions. However, gradients are usually ignored in tissue engineering, mainly for practical reasons, despite their physiological functions. Creating gradients, especially multiple gradients, remains challenging and often requires special equipment and a complex synthesis process.[6] Nevertheless, these last years, many techniques were established to create layered or continuous gradients in hydrogels.[6–14] The choice of the synthesis process is based on different criteria such as the type of gradients (*i.e.* continuous or layered), type of precursors (*i.e.* low or high viscosity, crosslinking mechanism), freedom of geometries (*i.e.* film, cylinder, or complex 3D printed geometry), or the number of gradients (*i.e.* gradient in one or different directions).

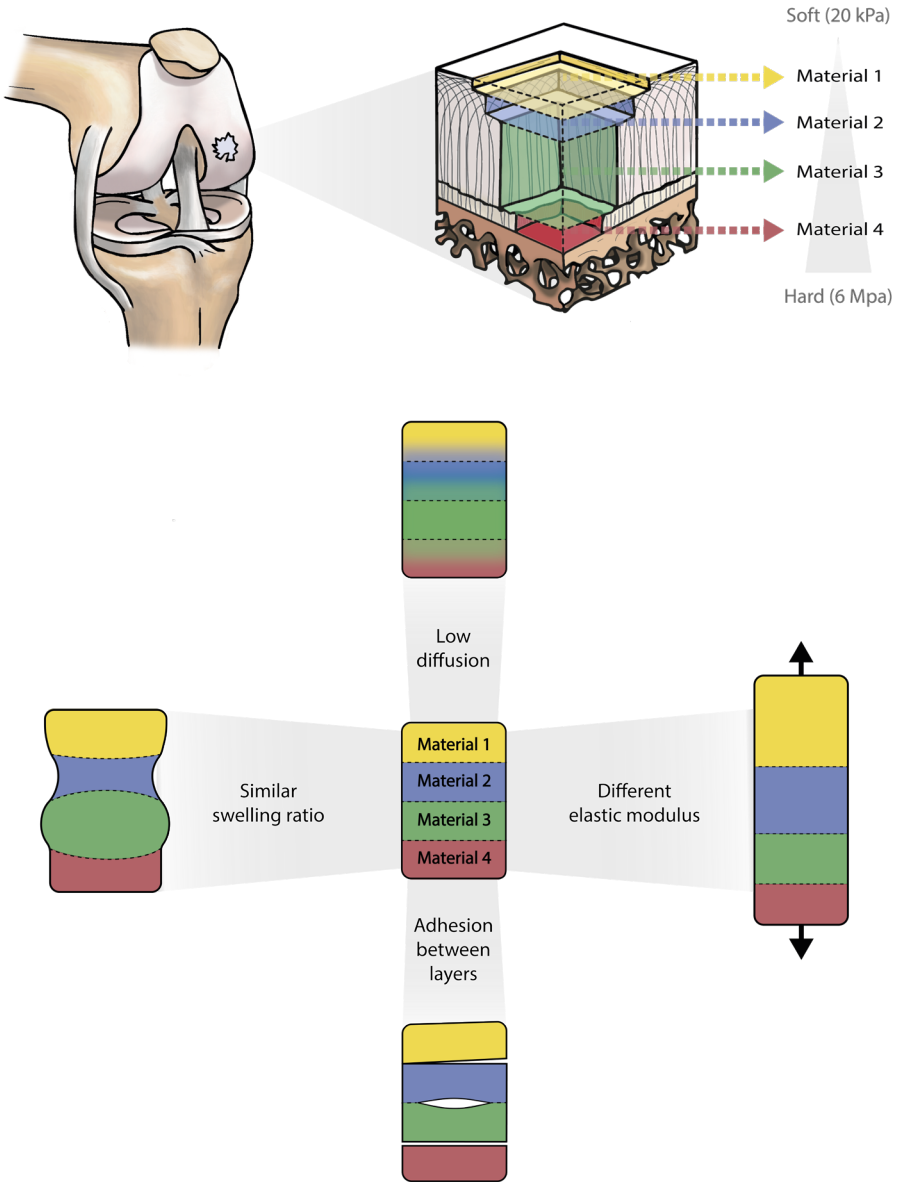

Fig. S9: Requirements for developing mechanical gradients in hydrogels through sequential layering. The example illustrates the local replacement of osteochondral tissues exhibiting a mechanical gradient with four different materials.

3. Supplementary movies

Movie 1: 3D projection showing the microstructure of a representative silk granular hydrogel ($4S^3$) observed with fluorescence confocal microscopy.
Movie_1-Microstructure_of_silk_granular_hydrogel.gif

Movie 2: Injectability of representative silk granular hydrogel precursors through a 16G needle.
Movie_2-Injectability_of_silk_granular_hydrogel_precursor.mp4

4. References

1 D. Chelazzi, D. Badillo-Sanchez, R. Giorgi, A. Cincinelli and P. Baglioni, *J. Colloid Interface Sci.*, 2020, **576**, 230–240.
2 N. Drnovšek, R. Kocen, A. Gantar, M. Drobnič-Košorok, A. Leonardi, I. Križaj, A. Rečnik and S. Novak, *J. Mater. Chem. B*, 2016, **4**, 6597–6608.
3 X. Wu, X. Wu, M. Shao and B. Yang, *Int. J. Biol. Macromol.*, 2017, **102**, 1202–1210.
4 Y. Srisuwan, P. Srihanam and Y. Baimark, *J. Macromol. Sci. Part A*, 2009, **46**, 521–525.
5 N. Jaramillo-Quiceno, C. Álvarez-López and A. Restrepo-Osorio, *Procedia Eng.*, 2017, **200**, 384–388.
6 C. Li, L. Ouyang, J. P. K. Armstrong and M. M. Stevens, *Trends Biotechnol.*, DOI:10.1016/j.tibtech.2020.06.005.
7 S. Xin, D. Chimene, J. E. Garza, A. K. Gaharwar and D. L. Alge, *Biomater. Sci.*, 2019, **7**, 1179–1187.
8 J. Guo, M. Liu, A. T. Zehnder, J. Zhao, T. Narita, C. Creton and C.-Y. Hui, *J. Mech. Phys. Solids*, 2018, **120**, 79–95.
9 S. E. Bakarich, R. Gorkin, R. Gately, S. Naficy, M. in het Panhuis and G. M. Spinks, *Addit. Manuf.*, 2017, **14**, 24–30.
10 L. M. Cross, K. Shah, S. Palani, C. W. Peak and A. K. Gaharwar, *Nanomedicine Nanotechnol. Biol. Med.*, 2018, **14**, 2465–2474.
11 J. He, T. Qin, Y. Liu, X. Li, D. Li and Z. Jin, *Mater. Lett.*, 2014, **137**, 393–397.
12 G. Xu, Z. Ding, Q. Lu, X. Zhang, X. Zhou, L. Xiao, G. Lu and D. L. Kaplan, *Protein Cell*, 2020, **11**, 267–285.
13 T. H. Kim, D. B. An, S. H. Oh, M. K. Kang, H. H. Song and J. H. Lee, *Biomaterials*, 2015, **40**, 51–60.
14 L. G. Major, A. W. Holle, J. L. Young, M. S. Hepburn, K. Jeong, I. L. Chin, R. W. Sanderson, J. H. Jeong, Z. M. Aman, B. F. Kennedy, Y. Hwang, D.-W. Han, H. W. Park, K.-L. Guan, J. P. Spatz and Y. S. Choi, *ACS Appl. Mater. Interfaces*, 2019, **11**, 45520–45530.